

# On the formation of direct collapse black hole seeds: Impact of gas spin and Lyman Werner flux

Aklant K. Bhowmick<sup>1</sup>, Laura Blecha<sup>1</sup>, Paul Torrey<sup>1</sup>, Luke Zoltan Kelley<sup>2</sup>,  
Mark Vogelsberger<sup>3</sup>, Dylan Nelson<sup>4</sup>, Rainer Weinberger<sup>5</sup>, Lars Hernquist<sup>5</sup>

<sup>1</sup>*Dept. of Physics, University of Florida, Gainesville, FL 32611, USA*

<sup>2</sup>*Dept. of Physics and Astronomy, Northwestern University, Evanston, IL 60208, United States*

<sup>3</sup>*Dept. of Physics, Kavli Institute for Astrophysics and Space Research, Massachusetts Institute of Technology, Cambridge, MA 02139, USA*

<sup>4</sup>*Universität Heidelberg, Zentrum für Astronomie, Institut für theoretische Astrophysik, Albert-Ueberle-Str. 2, 69120 Heidelberg, Germany*

<sup>5</sup>*Harvard-Smithsonian Center for Astrophysics, 60 Garden Street, Cambridge, MA 02138, USA*

16 March 2022

## ABSTRACT

Direct collapse models for black hole (BH) formation predict massive ( $\sim 10^5 M_\odot$ ) seeds, which hold great appeal as a means to rapidly grow the observed  $\sim 10^9 M_\odot$  quasars by  $z \gtrsim 7$ . However, the direct collapse of a pristine atomic cooling halo to a BH seed likely requires fine-tuned conditions. In this work, we use cosmological zoom simulations to study systematically the impact of requiring: 1) low gas angular momentum (spin), and 2) a minimum incident Lyman Werner (LW) flux radiation in order to form direct-collapse BH seeds. We start with a baseline model (introduced in Bhowmick et al. 2021) that restricts black hole seed formation (with seed masses of  $M_{\text{seed}} = 1.25 \times 10^4, 1 \times 10^5$  &  $8 \times 10^5 M_\odot/h$ ) to occur only in haloes with a minimum total mass ( $3000 \times M_{\text{seed}}$ ) and star forming, metal poor gas mass ( $5 \times M_{\text{seed}}$ ). When seeding is further restricted to halos with low gas spins (i.e. smaller than the minimum value required for the gas disc to be gravitationally stable), the number of seeds formed is suppressed by factors of  $\sim 6$  compared to the baseline model regardless of the mass threshold used. In contrast, imposing a minimum LW flux ( $> 10 J_{21}$ ) disproportionately suppresses seed formation in  $\lesssim 10^9 M_\odot/h$  halos, by factors of  $\sim 100$  compared to the baseline model. Very few BH merger events occur in the models with a LW flux criterion, and because early BH growth is dominated by mergers in our models, this results in only the most massive ( $8 \times 10^5 M_\odot/h$ ) seeds being able to grow to the supermassive regime ( $\gtrsim 10^6 M_\odot/h$ ) by  $z = 7$ . Our results therefore suggest that producing the bulk of the  $z \gtrsim 7$  BH population requires alternate seeding channels, early BH growth dominated by rapid or super-Eddington accretion, massive seeding scenarios that do not depend on incident LW flux, or a combination of these possibilities.

**Key words:** BHs: general, seeds

## 1 INTRODUCTION

Supermassive black holes (SMBHs) are now believed to be central components of galaxy formation and evolution. Almost every massive galaxy in the local Universe harbors a SMBH (Kormendy & Richstone 1992; Harms et al. 1994; Miyoshi et al. 1995). Evidence for SMBHs is also seen at higher redshifts ( $z \gtrsim 1$ ), where they are primarily observed as active galactic nuclei (AGN). The most luminous AGN (a.k.a quasars) have now been observed to redshifts of  $z \sim 7.5$  (Fan et al. 2001; Mortlock et al. 2011; Wu et al. 2015; Bañados et al. 2018). However, these quasars likely represent a very tiny and highly biased portion of the underlying SMBH population at  $z \gtrsim 7$ ; this population is going to be unveiled by upcoming facilities such as James Webb Space Telescope (JWST; Gardner et al. 2006), the Nancy Graham Roman Space telescope (NGRST, formerly WFIRST; Spergel et al.

2015), the Lynx X-ray Observatory (The Lynx Team 2018), and the Laser Interferometer Space Antenna (LISA; Baker et al. 2019). The overall  $z \gtrsim 7$  SMBH population (including the observed brightest quasars) potentially contains imprints of the earliest seeds of SMBHs, which is currently a major theoretical gap in contemporary galaxy formation models.

A popular candidate for SMBH seeds is the remnant of a first generation (Population III or Pop III) star (Madau & Rees 2001; Volonteri et al. 2003). This is a very promising channel for potentially explaining a substantial fraction of SMBHs, largely because they almost certainly exist as an inevitable consequence of the collapse of such massive stars ( $\sim 10 - 1000 M_\odot$ ). Seeds formed via this channel are predicted to have masses  $\sim 100 M_\odot$  (Fryer et al. 2001). However, the inferred masses of the  $z > 7$  quasars ( $\sim 10^9 M_\odot/h$ ) pose a huge challenge to Pop III seeds, since they require sustained accretion of gas at the Eddington limit to grow by

$\sim 7$  orders of magnitude by  $z \sim 7$ . Alternatively, a higher initial seed mass ( $\sim 10^4 - 10^6 M_\odot/h$ ) makes it substantially easier for BH seeds to grow to  $\gtrsim 10^9 M_\odot/h$  by  $z \sim 7$ . For this reason, black holes formed from direct collapse of pristine gas (a.k.a. “direct collapse black holes” or “DCBHs”) have become popular candidates for  $z > 7$  quasar progenitors, particularly because this channel can potentially form very massive seeds between  $\sim 10^4 - 10^6 M_\odot/h$  (Bromm & Loeb 2003; Begelman et al. 2006; Regan et al. 2014; Latif et al. 2016; Luo et al. 2018; Becerra et al. 2018; Wise et al. 2019; Luo et al. 2020).

In addition to a lack of metal-line cooling, a key requirement for this scenario is the absence of molecular hydrogen cooling, which can otherwise lead to fragmentation of gas into Pop III star forming regions. Molecular hydrogen formation can be suppressed if the gas is exposed to a sufficient amount of UV radiation in the Lyman Werner (LW) band (11.2 – 13.5 eV) sourced from nearby star forming regions, particularly young Population II (Pop II) and Pop III stars. The minimum amount of LW flux ( $J_{\text{crit}}$ ) required to suppress fragmentation is not well constrained, largely due to uncertainties in the source radiation spectrum (Latif et al. 2014), self shielding of  $H_2$  (Wolcott-Green et al. 2011) and the modeling of gas chemistry (Glover 2015). Accounting for these uncertainties, estimated values of  $J_{\text{crit}}$  have ranged from  $\sim 30 - 10^5 J_{21}$  (where  $J_{21} = 10^{-21} \text{ ergs}^{-1} \text{ cm}^{-2} \text{ Hz}^{-1} \text{ sr}^{-1}$ ) (Omukai 2001; Bromm & Loeb 2003; Shang et al. 2010). Recent works have also found that dynamical heating in halos (triggered by periods of rapid growth) can amplify the LW induced suppression of cooling, thereby further decreasing  $J_{\text{crit}}$  to  $\sim 3 J_{21}$  (Wise et al. 2019; Regan et al. 2020b).

Another potential impediment for DCBH formation is the angular momentum of the gas. In addition to the suppression of molecular hydrogen cooling, a large inflow rate ( $\gtrsim 0.1 M_\odot \text{ yr}^{-1}$  at a few tens of pc scales sustained for  $\sim 10$  Myr) is also needed to form a massive compact object at the center (Begelman 2010; Hosokawa et al. 2012, 2013; Schleicher et al. 2013; Regan et al. 2020a). Halos with high gas spin can provide rotational support to the pre-galactic gas disc and prevent the gas from achieving such high inflow rates.

While DCBHs are a promising alternative to alleviate the stringent growth timescales of lower mass ( $\lesssim 10^3 M_\odot$ ) seeds, the previous considerations make it clear that their formation requires a number of fairly stringent conditions to be simultaneously satisfied. This raises several broad questions: 1) How (un)common are DCBH forming gas environments within a given large scale structure? 2) What portion of the observable SMBH population originates from DCBH seeds?

Several aspects of these questions have been investigated in previous works; a vast majority of them use semi-empirical models (Lodato & Natarajan 2006, 2007; Natarajan & Volonteri 2012; Dijkstra et al. 2008, 2014; Ricarte & Natarajan 2018; DeGraf & Sijacki 2020). Lodato & Natarajan (2006) found that only  $\sim 5\%$  of dark matter halos ( $\sim 10^7 M_\odot$ ) have spins that are low enough to form DCBHs ( $\sim 10^5 M_\odot$ ). Dijkstra et al. (2008) found that a very small fraction of halos ( $10^{-8} - 10^{-6}$ ) may have LW fluxes ( $\gtrsim 10^3 J_{21}$ ) necessary to prevent fragmentation. Overall, these results indicate that DCBH formation sites may be rare. While they could potentially explain the rarest, brightest tip of the observed high- $z$  SMBH population, accounting for the “typical” (lower

masses and luminosities, yet to be observed) SMBHs at these redshifts but may be a lot more difficult.

Recently, cosmological hydrodynamic simulations (see Vogelsberger et al. 2020, for a recent review) have been used to probe the large scale structure for DCBH formation sites (Habouzit et al. 2016; Tremmel et al. 2017; Dunn et al. 2018; Luo et al. 2020; Chon et al. 2021). While they are considerably more expensive than semi-empirical models, they have the unique advantage of being able to self-consistently track the dynamics of gas which is a crucial ingredient for governing seed formation. This makes them an ideal tool to systematically assess the importance of different seeding criteria on DCBH formation. For example, Habouzit et al. (2016) (hereafter H16) studied the impact of varying  $J_{\text{crit}}$  using simulations spanning a wide range of volumes and resolutions. Dunn et al. (2018) performed a similar study, seeding DCBHs using only the local gas properties instead of those averaged over the entire host halo. In principle, the use of local gas properties is more physically consistent than halo averaged gas properties (as done in Bhowmick et al. 2021 where the seeding is based on the total mass and star forming, metal poor gas mass of a halo); this is particularly true for modeling seeding conditions such as high densities and low metallicities. However, the actual length scales that are referred to as “local” are determined by the spatial resolution of the simulation. Achieving resolution convergence may be more challenging when the seeding is only based on properties of a single “local” gas cell. Moreover, seeding conditions based on properties such as gas angular momentum inevitably require information beyond the local environment. Consequently, Dunn et al. (2018) decided not to explore the impact of gas angular momentum on seed formation. At the same time, H16 also decided to focus only on the LW flux criterion.

In this work, we use a suite of cosmological hydrodynamic zoom simulations to systematically characterize the impact of both Lyman Werner flux and gas angular momentum based seeding criteria on the SMBH population at  $z > 7$ . We specifically investigate how seeds of different birth masses grow in the presence of these seeding criteria. This enables us to assess the feasibility of DCBH channels to explain different parts of the underlying mass function of  $z > 7$  SMBHs. This work is part of a larger effort (started with Bhowmick et al. 2021) to build a family of gas based seeding prescriptions for the next generation of cosmological simulations. Our prescriptions are generally agnostic about which theoretical seed formation channels they may represent (e.g., Pop III, DCBH or something else), such that we can tune our parameters to emulate a specific model. To that end, we use zoom simulations to characterize the impact of various aspects of galaxy evolution on the formation of seeds and their subsequent growth.

This paper is organized as follows. Section 2 presents the basic methodology, which includes the simulation suite, and the implementation and gas angular momentum and LW flux based seeding. Section 3 describes the results of our work, followed by our main conclusions in Section 4.

## 2 METHODS

Our simulations were run using the AREPO code (Springel 2010; Pakmor et al. 2011, 2016; Weinberger et al. 2020)

which solves for gravity coupled with magnetohydrodynamics (MHD). The gravity sector involves an N-body solver using PM-Tree method (Barnes & Hut 1986). The MHD sector uses a quasi-Lagrangian description of the gas fluid with an unstructured grid constructed via a Voronoi tessellation of the domain. AREPO has been used to run a variety of cosmological simulations which include uniform volumes such as Illustris (Vogelsberger et al. 2014; Genel et al. 2014; Nelson et al. 2015; Sijacki et al. 2015), IllustrisTNG (Pillepich et al. 2018b; Nelson et al. 2018; Marinacci et al. 2018; Naiman et al. 2018; Springel et al. 2018; Pillepich et al. 2019; Nelson et al. 2019a,b), and zoom volumes such as AURIGA (Grand et al. 2017) and HESTIA (Libeskind et al. 2020).

AREPO contains several distinct sets of galaxy formation models. As in Bhowmick et al. (2021), we use the IllustrisTNG model (Weinberger et al. 2017; Pillepich et al. 2018a) in this work as our baseline (except for the BH seed model). The key features of the IllustrisTNG model include: star formation in the dense interstellar medium, where stars form stochastically from gas cells (with an associated time scale of 2.2 Gyr) when their densities exceed a threshold of  $\rho_{\text{SF}} = 0.13 \text{ cm}^{-3}$ , and the ISM itself is modelled by an effective equation of state (Springel & Hernquist 2003; Vogelsberger et al. 2013). Subsequent stellar evolution and metal enrichment assumes a Chabrier (2003) initial mass function for the underlying single stellar populations (SSPs) represented by the star particles. Metal cooling is implemented in the presence of a spatially uniform and time dependent ultraviolet background (UVB) radiation field (including the self-shielding of dense gas). A uniform seed magnetic field ( $10^{-14}$  comoving Gauss) is added at an arbitrary orientation, and its subsequent evolution is governed by MHD.

The modelling of black hole seeding is discussed in detail in the following section. Here, we summarize the other aspects of the black hole modeling that have been kept the same as IllustrisTNG. Once seeded, BHs can grow either via gas accretion or mergers with other BHs. BH accretion follows the Eddington limited Bondi-Hoyle formula and is given by

$$\dot{M}_{\text{BH}} = \min(\dot{M}_{\text{Bondi}}, \dot{M}_{\text{Edd}}) \quad (1)$$

$$\dot{M}_{\text{Bondi}} = \frac{4\pi G^2 M_{\text{BH}}^2 \rho}{c_s^3} \quad (2)$$

$$\dot{M}_{\text{Edd}} = \frac{4\pi G M_{\text{BH}} m_p}{\epsilon_r \sigma_T} c \quad (3)$$

where  $G$  is the gravitational constant,  $M_{\text{BH}}$  is the mass of the BH,  $\rho$  is the local gas density,  $c_s$  is the local sound speed of the gas,  $m_p$  is the mass of the proton,  $\epsilon_r$  is the radiative efficiency and  $\sigma_T$  is the Thompson scattering cross section. The resulting bolometric luminosity is given by

$$L = \epsilon_r \dot{M}_{\text{BH}} c^2, \quad (4)$$

where  $\epsilon_r = 0.2$ . Accreting BHs inject energy into the surrounding gas as Active Galactic Nuclei (AGN) feedback; this is implemented in two modes. For Eddington ratios ( $\eta \equiv \dot{M}_{\text{bh}}/\dot{M}_{\text{Edd}}$ ) higher than a critical threshold of  $\eta_{\text{crit}} = \min[0.002(M_{\text{BH}}/10^8 M_{\odot})^2, 0.1]$ , thermal energy is injected into the neighboring gas at a rate given by  $\epsilon_{f,\text{high}} \epsilon_r \dot{M}_{\text{BH}} c^2$ , where  $\epsilon_{f,\text{high}} \epsilon_r = 0.02$ ;  $\epsilon_{f,\text{high}}$  is referred to as the “high accretion state” coupling efficiency. For Eddington ratio values lower than the critical threshold, kinetic energy is injected into the gas surrounding the black hole, in a time pulsed

fashion, as a directed ‘wind’ oriented along a randomly chosen direction; the energy injection rate ( $\dot{E}_{\text{kin}}$ ) is given by

$$\dot{E}_{\text{kin}} = \epsilon_{f,\text{kin}} \dot{M}_{\text{BH}} c^2, \quad (5)$$

$$\epsilon_{f,\text{kin}} = \min\left(\frac{\rho}{\rho_{\text{SF}}}, 0.2\right). \quad (6)$$

The merging of BH pairs occurs when their separations fall below the smoothing length of the BHs; this is the minimum radius of a sphere that encloses a specified number of neighboring gas cells weighted over a smoothing kernel. Due to the limited resolution, the small-scale dynamics of BHs cannot be determined self-consistently; this is particularly true when the BH mass is smaller than the mass of the DM particles. To avoid spurious forces, the BHs are therefore re-positioned to the location of the closest potential minimum.

## 2.1 Modelling of black hole seeds

Our seed models are based on the gas properties of halos and are designed to emulate conditions for DCBH seed formation. We first apply a set of seeding criteria to restrict the seeding to halos with pristine star forming gas. In particular, seeds of mass  $M_{\text{seed}}$  are allowed to form only in halos which satisfy:

- a minimum threshold for star forming, metal poor gas mass, denoted by  $\tilde{M}_{\text{sf,mp}}$ . As in Bhowmick et al. (2021), the tilde indicates that the mass threshold is a dimensionless quantity normalized to the seed mass:  $\tilde{M}_{\text{sf,mp}} \equiv M_{\text{sf,mp}}/M_{\text{seed}}$ . ‘Metal poor’ gas cells refer to those with metallicities less than  $10^{-4} Z_{\odot}$ . Note however that our results are not significantly sensitive to the choice of this threshold from  $10^{-5} - 10^{-2} Z_{\odot}$ .
- a minimum threshold for the total mass, denoted by  $\tilde{M}_h$  (this is also a dimensionless quantity normalized to the seed mass:  $\tilde{M}_h \equiv M_h/M_{\text{seed}}$ ).

A range of models with the above seeding criteria (in the parameter space of  $\tilde{M}_{\text{sf,mp}}$ ,  $\tilde{M}_h$  and  $M_{\text{seed}}$ ) has been explored in Bhowmick et al. (2021), where we found that both  $\tilde{M}_{\text{sf,mp}}$  and  $\tilde{M}_h$  leave strong and distinct imprints on the merger rates, and therefore also the BH masses. More specifically, a factor of 10 increase in  $\tilde{M}_h$  causes  $\sim 100$  times suppression of merger rates at  $z > 15$ ;  $\tilde{M}_{\text{sf,mp}}$  has greater impact at lower redshifts ( $z \sim 7 - 15$ ), where it can suppress the merger rates by factors of  $\sim 8$  when increased from 5 to 150.

In this work, we fix  $\tilde{M}_h = 3000$ ,  $\tilde{M}_{\text{sf,mp}} = 5$  and explore seed masses of  $M_{\text{seed}} = 1.25 \times 10^4, 1 \times 10^5, 8 \times 10^5 M_{\odot}/h$ ; this is motivated by a number of considerations. First, the seed masses and the corresponding halo masses for their formation ( $\sim 10^7 - 10^9 M_{\odot}/h$  halos) are consistent with theoretical predictions for where DCBHs are expected to form (Bromm & Loeb 2003; Koushiappas et al. 2004). Second, the choice of  $\tilde{M}_h = 3000$ ,  $\tilde{M}_{\text{sf,mp}} = 5$  provides reasonably well converged results with respect to increasing resolution (Bhowmick et al. 2021). Third, this model also produces a sufficient number of BHs within our zoom volume (to be described in Section 2.2), so that we can put in additional criteria to further restrict the seeding and investigate their impact. Hereafter, we shall refer to the above criterion as the *baseline seeding criteria*.

Having applied the baseline seeding criteria, we then explore the impact of further restricting the seeding based on the gas angular momentum and LW flux as described in the following subsections.

### 2.1.1 Gas spin criterion

Here, we restrict the seeding to halos with low gas angular momentum. For each halo, we compute the net angular momentum of all gas cells with respect to their center of mass, which we hereafter refer to as “gas spin” ( $\vec{J}_{\text{spin}}$ ), as

$$\vec{J}_{\text{spin}} = \sum_i^{\text{gas cells}} [\vec{r}_i \times \vec{p}_i - \vec{r}_{\text{com}} \times \vec{p}_{\text{com}}] \quad (7)$$

where the summation is over all gas cells around the halo potential minimum up to the halo virial radius  $R_{\text{vir}}$ ;  $\vec{r}_i$  and  $\vec{p}_i$  are the position and momentum of the  $i^{\text{th}}$  gas cell.  $\vec{r}_{\text{com}}$  and  $\vec{p}_{\text{com}}$  are the position and momentum of the center of mass of gas cells within the virial radius. We define the dimensionless gas spin parameter of the halo as

$$\lambda = \frac{|\vec{J}_{\text{spin}}|}{\sqrt{2} M_{\text{gas}} R_{\text{vir}} V_{\text{vir}}} \quad (8)$$

where  $M_{\text{gas}}$  is total gas mass within the halo virial radius, and  $V_{\text{vir}} = \sqrt{\frac{GM_{\text{vir}}}{R_{\text{vir}}}}$  is the circular velocity.

Our gas spin criterion is motivated by the results of [Lodato & Natarajan \(2006\)](#) on the stability analysis of pre-galactic gas discs in high redshift halos (as also adopted by [Natarajan & Volonteri 2012](#) and [DeGraf & Sijacki 2020](#)). They derive a maximum gas spin  $\lambda_{\text{max}}$ , above which the gas disc is gravitationally stable. At lower gas spins, the disc becomes prone to gravitational collapse, potentially resulting in a massive DCBH seed. This maximum gas spin is given by

$$\lambda_{\text{max}} = \frac{m_d^2 Q_c}{8 j_d} (T_{\text{vir}}/T_{\text{gas}})^{1/2} \quad (9)$$

where  $m_d$  and  $j_d$  are the fractions of the mass and angular momentum respectively, of the halo that forms the disc.  $Q_c$  is the Toomre instability parameter.  $T_{\text{vir}}$  is the virial temperature of the halo and  $T_{\text{gas}}$  is the mean gas temperature. When  $\lambda < \lambda_{\text{max}}$ , the fraction of the disk mass that falls towards the center (providing fuel for BH seed formation) is  $\sqrt{1 - \lambda/\lambda_{\text{max}}}$ .

We now focus on the implications of the foregoing physical arguments on our seed models. For a given seed mass  $M_{\text{seed}}$  to form, halos must have: 1) a gravitationally unstable disk and 2) a sufficient amount of gas mass ( $> M_{\text{seed}}$ ) collapsing to the center as a consequence. This corresponds to the following seeding criteria:

$$\lambda < \lambda_{\text{max}} \quad (10)$$

and

$$M_h > \frac{M_{\text{seed}}}{m_d \sqrt{1 - \lambda/\lambda_{\text{max}}}} \quad (11)$$

where  $M_h$  is the halo mass. As it turns out, Eq. (11) corresponds to halo mass thresholds which typically lie between  $\sim 100 - 500 M_{\text{seed}}$ , which is much smaller than our baseline criteria for halo mass ( $\tilde{M}_h = 3000$ ). Therefore, it is only Eq. (10) that impacts our seeding.

To determine  $\lambda_{\text{max}}$  we compute  $T_{\text{vir}}$  and  $T_{\text{gas}}$  for every halo on the fly during the simulation. The parameters  $m_d$ ,  $j_d$  and  $Q_c$  can depend on the structure of disks, which may not be well resolved for all of our simulations, particularly in low mass halos at early epochs. Computing these quantities on the fly would also be computationally demanding.

For these reasons we instead simplify our model by assuming  $m_d = j_d = 0.05$  and  $Q_c = 2$ , as also done in [Natarajan & Volonteri 2012](#) and [DeGraf & Sijacki \(2020\)](#). We test the choices for  $m_d$  and  $j_d$  using one of our highest resolution simulations (gas mass resolutions  $\sim 10^3 M_{\odot}/h$ ), where we compute them in post-processing for our DCBH forming halos using a kinematic decomposition of gas cells (as done in [Huang et al. 2018](#)); the values tend to lie between 0.01 to 0.1, broadly consistent with our assumed value of 0.05. Hereafter, we shall refer to Eq. (10) as the *gas spin criterion*.

### 2.1.2 Lyman Werner (LW) flux criterion

We also examine the impact of restricting the seeding to halos exposed to a LW flux above a critical threshold. We first describe our methodology to compute the LW flux over the entire simulation box. Note that our simulations do not include direct radiative transfer. Therefore, we adopt an empirical prescription developed in [Agarwal et al. \(2012\)](#) and [Agarwal et al. \(2014\)](#) to compute the LW flux on the fly. This prescription assumes a template SED for Pop III stars adopted from [Schaerer \(2002\)](#); for Pop II stars, the SED was derived using the STARBURST99 stellar population synthesis code ([Leitherer et al. 1999](#)).

In principle, the LW flux at a given location consists of a background component (originating from distant stars not necessarily within the simulation volume) and a spatially varying component (originating from nearby stars). The background component depends on the global star formation rate density, and is estimated to be  $0.01 J_{21}$  at  $z \sim 25$  to  $1 J_{21}$  at  $z \sim 7 - 10$  ([Johnson et al. 2013](#)). The spatially varying component can however be much higher than the background component, particularly at the sites of potential seed formation. Moreover, the flux thresholds we plan to consider are also  $\sim 10 - 300$  times higher. Therefore, we neglect the background component and include only the spatially varying component in our calculation (as also done in [Habouzit et al. 2016](#)). The spatially varying components for the Pop III and Pop II LW fluxes (adopted from [Agarwal et al. 2014](#)) are given by

$$J_{\text{LW}}^{\text{III}} = 15 \times \sum_i \left( \frac{r_i^2}{1 \text{ kpc}} \right) \left( \frac{m_{*,i}}{10^3 M_{\odot}} \right) \quad (12)$$

and

$$J_{\text{LW}}^{\text{II}} = 3 \times \sum_i \left( \frac{r_i^2}{1 \text{ kpc}} \right) \left( \frac{m_{*,i}}{10^3 M_{\odot}} \right) \quad (13)$$

respectively, where  $m_{*,i}$  is the mass of each resolution element comprised of young stars,  $r_i$  is the corresponding distance.

In our simulations, we compute the LW flux at the locations of all gas cells, by adding up the contributions from nearby star forming gas. Each star forming gas cell is assumed to contain a single stellar population (SSP) characterized by its age and metallicity. We are interested in cells representing Pop III and Pop II SSPs, which are classified by metallicities of  $Z < 0.001 Z_{\odot}$  and  $0.001 < Z < 0.1 Z_{\odot}$ , respectively. Star-forming gas with  $Z > 0.1 Z_{\odot}$  does not contribute to our Lyman Werner flux calculation. Additionally, we include contributions only from star formation within the previous 5 Myr (consistent with [Agarwal et al. 2012, 2014](#); [DeGraf & Sijacki 2020](#)), since most LW photons are emitted within this



time interval due to the shorter lifetimes of the most massive Pop II and Pop III stars and the age dependence of their spectral energy distributions (Leitherer et al. 1999; Schaerer 2002). In a nutshell,  $m_{*,i}$  in Eqs. (12) and (13) is given by,

$$m_{*,i} = \text{SFR}_i \times 5 \text{ Myr} \quad (14)$$

where  $\text{SFR}_i$  is the star formation rate of the  $i^{\text{th}}$  gas cell.

For seeding BHs based on the calculated LW fluxes, we assume a threshold LW flux (Pop II + Pop III contribution) required for seeding, denoted by  $J_{\text{LW}}^{\text{min}}$ . The seeding criteria is then given by

$$M_{\text{LW}} > M_{\text{seed}} \quad (15)$$

where  $M_{\text{LW}}$  is the total mass of gas cells within a given halo that are exposed to LW fluxes greater than  $J_{\text{LW}}^{\text{min}}$ .

## 2.2 Simulation suite

Our simulation suite consists of a series of zoom simulations of a universe with an underlying cosmology adopted from Planck Collaboration et al. (2016), ( $\Omega_{\Lambda} = 0.6911, \Omega_m = 0.3089, \Omega_b = 0.0486, H_0 = 67.74 \text{ km sec}^{-1} \text{ Mpc}^{-1}, \sigma_8 = 0.8159, n_s = 0.9667$ ). The initial conditions (ICs) are generated using MUSIC (Hahn & Abel 2011) within a parent box with  $(25 \text{ Mpc}/h)^3$  comoving volume.

Our density field realization and the zoom-in region of interest is the same as that of Bhowmick et al. (2021). Here we briefly summarize the main features and refer the interested reader to Bhowmick et al. (2021) for more details. We first ran a uniform volume simulation with  $128^3$  particles and selected a target halo of mass  $3.5 \times 10^{11} M_{\odot}/h$  (corresponding to a peak height  $\nu = 3.3$ ) at  $z = 5$  to resimulate at higher resolutions. DM particles comprising that halo were traced to  $z = 127$ , wherein a cuboidal region enclosing these particles is selected for the zoom runs; this region was referred to as ZOOM\_REGION\_z5 in Bhowmick et al. (2021).

For our zoom-in ICs, the resolution of the zoom region is characterized by the parameter  $L_{\text{max}}$ , corresponding to a uniform box with  $2^{L_{\text{max}}}$  DM particles per side. Table 1 summarizes the mass and spatial resolutions in our zoom region for different values of  $L_{\text{max}}$ . The background grid is always kept at  $L_{\text{min}} = 7$ , while for the zoom region we explored  $L_{\text{max}} = 10, 11, 12$  and found that our results are reasonably well converged by  $L_{\text{max}} = 11$  (see Appendix A1). Therefore, we primarily use  $L_{\text{max}} = 11$  for this study.

### 2.2.1 Black hole seed models explored

Here we summarize the gas based seed models explored in this work. The key parameters of interest in our modelling are  $\tilde{M}_h, \tilde{M}_{\text{sf,mp}}, M_{\text{seed}}$  &  $J_{\text{LW}}^{\text{min}}$ . In addition, we have the gas spin criterion which can be switched on or off. As discussed in Section 2.1,  $\tilde{M}_h$  and  $\tilde{M}_{\text{sf,mp}}$  (which were explored in Bhowmick et al. 2021) are kept fixed at 3000 and 5, respectively.

When exploring models with the LW flux criterion, we consider  $J_{\text{LW}}^{\text{min}}$  values 10, 50 & 300  $J_{21}$ , which are well within the current uncertainty in the threshold LW flux required to suppress molecular hydrogen cooling ( $J_{\text{LW}} \sim 1 - 10^5 J_{21}$ ). Given the size of our zoom volume, we are not able to probe threshold LW fluxes higher than 300  $J_{21}$ . The  $M_{\text{seed}}$  values explored in this work are  $1.25 \times 10^4, 1 \times 10^5$  &  $8 \times 10^5 M_{\odot}/h$ , which broadly span the masses of DCBHs postulated by theory.

We use the following nomenclature to refer to our models for the remainder of this work. If a particular model only applies the baseline seeding criteria, we label it as ‘BASELINE’. When the gas spin criteria is included, we label it as ‘LOWSPIN’. When the LW flux criterion is included, then we include ‘LW\*’ where ‘\*’ is replaced by the  $J_{\text{LW}}^{\text{min}}$  flux value. For example,  $J_{\text{LW}}^{\text{min}} = 10$  would correspond to ‘LW10’.

## 3 RESULTS

### 3.1 Build up of DCBH formation sites

Figure 1 visualizes the evolution of the key properties of the gas distribution of the zoom region that drive the formation of the DCBHs, which proceeds as follows. As time progresses (Figure 1 shows  $z = 13$  to  $z = 7$ ) gravitational collapse and gas cooling leads to regions with densities high enough to trigger star formation (Figure 1: 1st row). Subsequent stellar evolution processes lead to a significant amount of metal enrichment (Figure 1: 2nd row). These earliest stages of star formation and metal enrichment regions are primarily comprised of young Pop III and Pop II stellar populations, which bombard nearby gas with LW radiation.

The LW fluxes from Pop II and Pop III stars are shown in the 3rd and 4th rows of Figure 1. We can see that the gas illuminated by Pop III stars is more evenly distributed through the simulation volume while the gas illuminated by Pop II stars is concentrated in regions with relatively higher metallicities. The BH seeds start forming in regions illuminated by LW flux. However, the metal enrichment substantially slows down the formation of new BHs after  $z \lesssim 11$ . Overall, the dispersion of metals as well as LW photons are two competing processes that are simultaneously driven by star formation; as a result, the window for DCBH formation is relatively narrow.

It is instructive to compare the impact of young Pop II vs. Pop III stars (age  $< 5 \text{ Myr}$ ) on DCBH seed formation in our models. Figure 2 shows the total amount of young stellar content in the form of Pop II and Pop III stars, as a function of redshift. At  $z \sim 16 - 20$ , the young stellar content is dominated by Pop III stars; this is because at this relatively early stage of star formation, a majority of the star forming regions have not yet been enriched by metals. However, by  $z \sim 7 - 15$ , the gas is sufficiently enriched and Pop II stars start to dominate the young stellar population.

Figure 3 compares the contributions from Pop III vs. Pop II stars to the LW fluxes on the surrounding gas. As expected from the results of Figure 2, we find that at  $z \sim 7 - 15$ , the LW flux is predominantly contributed by Pop II stars. Notably, even at  $z \sim 19$  where Pop III stars are more abundant overall, LW fluxes from Pop II stars still dominate at the highest values ( $\gtrsim 5 J_{21}$ ) relevant for BH formation. This is because the highest LW fluxes naturally occur in the densest regions, where metal enrichment (and therefore, Pop II star formation) is expected to be more prevalent compared to other locations. These findings are overall consistent with H16, where the contributions from Pop III stars is neglected in the LW flux calculation.

$L_{\max}$	$M_{dm} (M_{\odot}/h)$	$M_{gas} (M_{\odot}/h)$	$\epsilon (kpc/h)$	$M_{seed} (M_{\odot}/h)$	values explored
10	$1 \times 10^6$	$\sim 10^5$	0.5	$8 \times 10^5, 1 \times 10^5$	
11	$1.3 \times 10^5$	$\sim 10^4$	0.25	$8 \times 10^5, 1 \times 10^5, 1.25 \times 10^4$	
12	$1.6 \times 10^4$	$\sim 10^3$	0.125	$8 \times 10^5, 1 \times 10^5, 1.25 \times 10^4$	

**Table 1.** Spatial and mass resolutions within the zoom region of our simulations for various values of  $L_{\max}$  (see Section 2.2 for the definition).  $M_{dm}$  is the mass of a dark matter particle,  $M_{gas}$  is the typical mass of a gas cell (note that gas cells can refine and de-refine depending on the local density) and  $\epsilon$  is the gravitational smoothing length. The 4th column corresponds to the seed masses allowed at each  $L_{\max}$ , which is limited by the gas mass resolution.

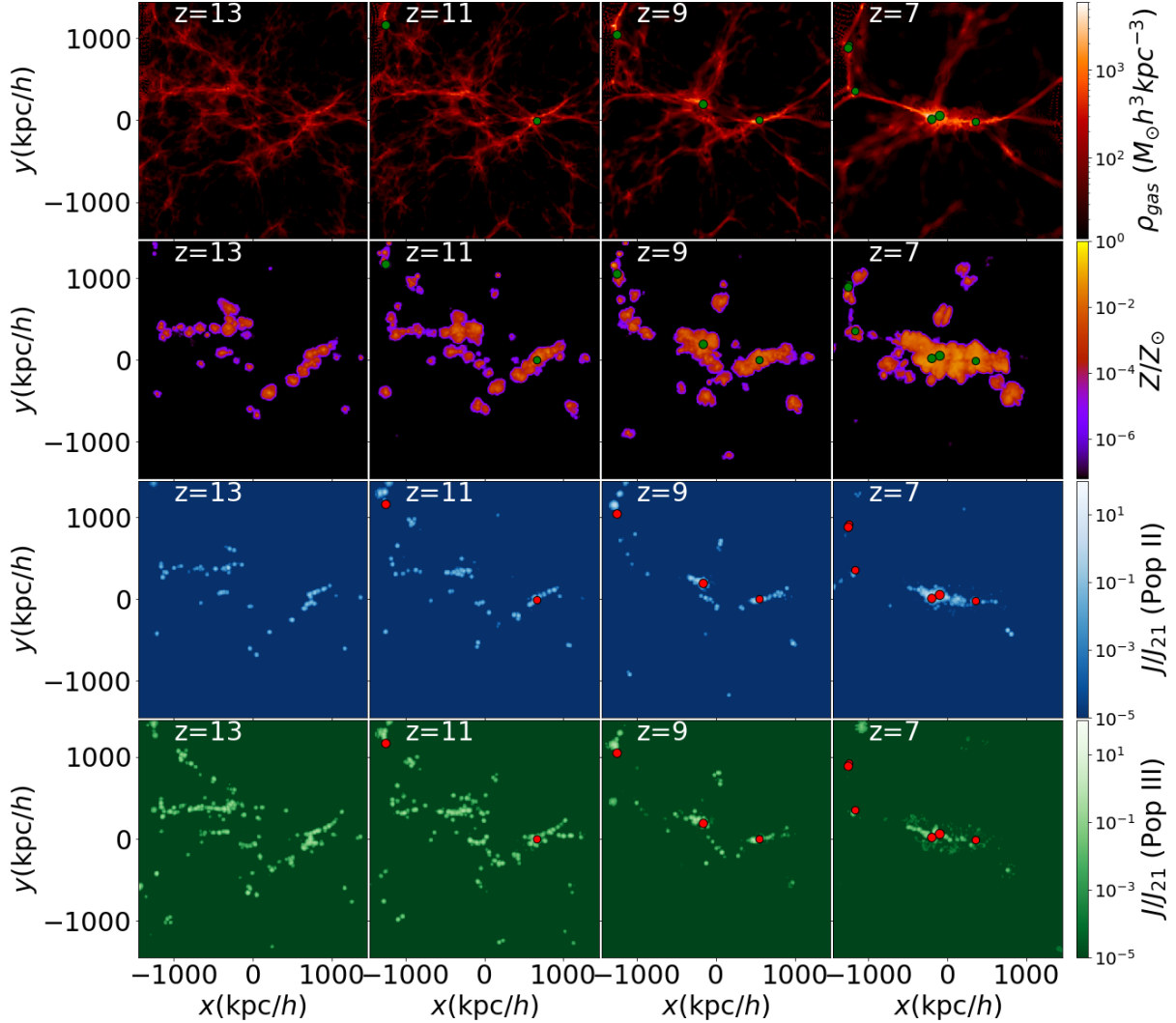


**Figure 1.** 2D projected color maps of the gas density (1st row), gas metallicity (2nd row) and Lyman Werner Fluxes from Pop II (3rd row) and Pop III (4th row) stars in our zoom region. Left to right panels show the redshift evolution from  $z = 13$  to  $z = 7$ . The green and red circles represent BHs seeded at  $1 \times 10^5 M_{\odot}/h$  in haloes with  $\bar{M}_h = 3000$ ,  $\bar{M}_{sf,mp} = 5$  and  $J_{LW}^{\min} = 10 J_{21}$ . As time evolves, the star forming and metal enriched regions appear throughout our zoom volume. These regions are sources of Lyman Werner photons. Seed black holes are formed in pristine star forming regions with sufficiently high Lyman Werner flux.

### 3.2 Characterizing halo properties relevant for DCBH formation

In this section, we look at the  $z \gtrsim 7$  halo population in the zoom region and characterize it in terms of properties that are relevant for DCBH formation. In particular, we consider the total mass, star forming, metal poor gas mass, gas spin, and LW fluxes of halos in Figure 4. Note here that we only

show halos where  $\lesssim 1\%$  of the total mass is contaminated by low resolution DM particles.

We first focus on how these different halo properties correlate with the halo mass for the overall population. The first row in Figure 4 shows that the star forming, metal poor gas mass positively correlates with the halo mass, particularly at  $z \gtrsim 11$  (at  $z = 7$ , there are too few metal poor halos

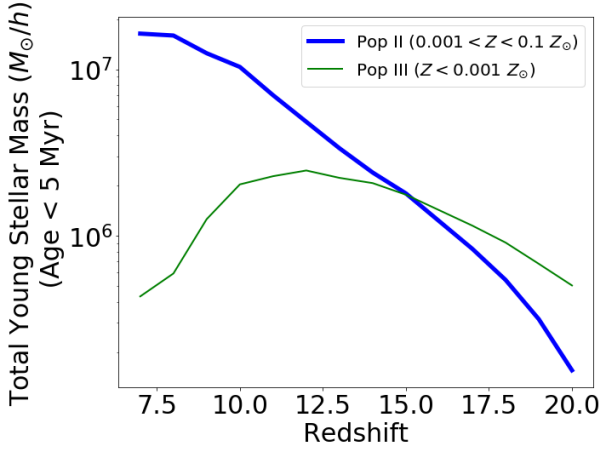


**Figure 2.** Total mass of young stars (age < 5 Myr) in the zoom region for Pop III ( $Z < 0.001 Z_{\odot}$ ; green curve) and Pop II ( $0.001 < Z < 0.1 Z_{\odot}$ ; blue curve) components. We find that between these components, Pop III stars dominate at  $z \gtrsim 15$  and Pop II stars dominate at  $z \sim 7 - 15$  (when most BHs are seeded).

in our volume to make definitive conclusions). This is not unexpected given that more massive halos also have higher gas content overall and typically have higher gas densities at their potential minima. That being said, metal enrichment will also be more prevalent in more massive star forming halos, thereby weakening the correlation; we can clearly see this happening for the most massive halos at  $z \gtrsim 11$ .

The dimensionless gas spin (shown in 2nd and 3rd rows of Figure 4) does not strongly correlate with halo mass. The gas spins are similar to those of the underlying dark matter spins, with mean values close to  $\sim 0.03 - 0.05$  at all halo masses and redshifts. These results are consistent with previous work using N-body simulations (Bullock et al. 2001; Macciò et al. 2007; Bett et al. 2007, 2010) as well as hydrodynamic simulations (Danovich et al. 2015; Zjupa & Springel 2017; DeGraf & Sijacki 2020). In addition, the lack of halo mass vs. spin correlation is also a natural prediction from tidal torque theory (see review by Schäfer 2009).

The last row of Figure 4 shows that more massive halos are exposed to higher LW fluxes. This is also expected as more massive halos typically have higher amounts of star formation overall; additionally, they spatially cluster more strongly with other massive star forming halos.

We now focus on the halo subsamples that satisfy different combinations of seeding criteria described in Section 2.1. The middle rows of Figure 4 show that most halos satisfying the baseline seeding criteria do not satisfy the gas spin criterion (filled red vs. open green circles). At  $z = 11$ , for instance, only  $\sim 13\%$  of halos satisfying the baseline seeding criteria also satisfy the gas spin criterion. This implies that gas angular momentum should have a significant impact on seed formation. Next, we see in the bottom row of Figure 4 that an even smaller fraction of halos ( $\sim 6\%$ ) satisfying the baseline criterion, also satisfy the LW flux criterion (filled blue vs open green circles). This suggests that the LW flux criterion may be even more stringent than the gas spin criterion. While Figure 4 shows the results for  $M_{\text{seed}} = 1 \times 10^5 M_{\odot}/h$ , the same inferences hold for all seed masses considered in this work.

### 3.3 Impact of gas spin and LW flux on BH seeding

We now quantify the impact of gas spin and LW flux criteria on the frequency of BH seeding. Figure 5 shows the number of seeds formed versus redshift, comparing the baseline model with the models in which a gas spin and/or LW flux criterion is added. Let us first focus on the gas spin criterion (solid vs. dashed lines of same color in upper panels of Figure 5). At the highest redshifts ( $z \gtrsim 20$ ), adding the gas spin criterion does not lead to any significant suppression in the number of seeds compared to the baseline seeding criteria; this is likely because at these early epochs, there has not been enough build up of angular momentum in the gas to prevent seeding. As we approach lower redshifts, the suppression due to gas spin criterion becomes stronger. At  $z \sim 11 - 12$  (where most seeds are produced), the gas spin criterion suppresses the number of seeds by factors of  $\sim 6$ . Lastly, the suppression is similar for all seed masses between  $1.25 \times 10^4 - 8 \times 10^5 M_{\odot}/h$ . These results are overall consistent with our findings in Section 3.2.

We now compare our results to previous work. Lodato & Natarajan (2006) used their empirical model to predict that  $\sim 5\%$  of halos with  $\sim 10^7 M_{\odot}$  have low enough spins to form  $\sim 10^5 M_{\odot}$  seed BHs (this percentage increases with halo mass). In our model, an overall suppression by factors of  $\sim 6$  implies that about 16% of halos satisfying the baseline criteria will actually be seeded with BHs once the gas spin criterion is applied. However, the threshold halo masses in our baseline model ( $> 3 \times 10^8 M_{\odot}/h$  for  $\sim 10^5 M_{\odot}$ ) are significantly higher than that in Lodato & Natarajan (2006) ( $10^7 M_{\odot}/h$ ). If we reduce the halo mass threshold to  $10^7 M_{\odot}$ ,  $\sim 6\%$  of our halos satisfy the gas spin criterion, in good agreement with this previous work.

Next, we quantify the suppression of seeding caused by the LW flux criterion (see Figure 5: lower panels). We first compare the less stringent LW criterion ( $J_{\text{LW}}^{\text{min}} = 10 J_{21}$ ) to the baseline model. The impact is strongest for the lowest halo mass thresholds corresponding to the lowest seed masses of  $M_{\text{seed}} = 1.25 \times 10^4 M_{\odot}/h$ ; in these systems, the number of seeds is suppressed by factors up to  $\sim 100$ . This reflects the fact that only the most massive halos ( $\sim 10^9 - 10^{10} M_{\odot}/h$ ) are typically exposed to LW fluxes  $\gtrsim 10 J_{21}$ . As a consequence, the LW flux criterion preferentially prevents seeding in the lower mass halos ( $\lesssim 10^9 M_{\odot}/h$ ) that would otherwise have formed low-mass seeds (this is seen more clearly in Figure 6). For the higher halo mass thresholds corresponding to seed masses of  $M_{\text{seed}} = 1 \times 10^5 M_{\odot}/h$  and  $8 \times 10^5 M_{\odot}/h$ , the numbers of seeds are suppressed by smaller factors of  $\sim 10$  and  $\sim 3$ , respectively.

When the LW flux is further increased from  $10 J_{21}$  to  $300 J_{21}$  (blue vs green lines in Figure 5: lower panels), the number of seeds is suppressed by factors up to  $\sim 30$  for  $1.25 \times 10^4 M_{\odot}/h$  seeds, and by factors up to  $\sim 8 - 10$  for  $1 \times 10^5 M_{\odot}/h$  seeds (note however that statistical uncertainties are large for  $J_{\text{LW}}^{\text{min}} = 300 J_{21}$ ). We can compare the results on the impact of LW flux threshold to predictions from hydrodynamic simulations of H16; they find a  $\sim 100$  times decrease in the number densities of halos with critical LW fluxes varying from 30 to  $300 J_{21}$ . Notably, the impact of LW flux in our models is somewhat smaller than that of H16; there are several factors that can contribute to this. Firstly, note that the simulation volume in H16 (142 Mpc/h box size) is significantly larger than our zoom volume; there-

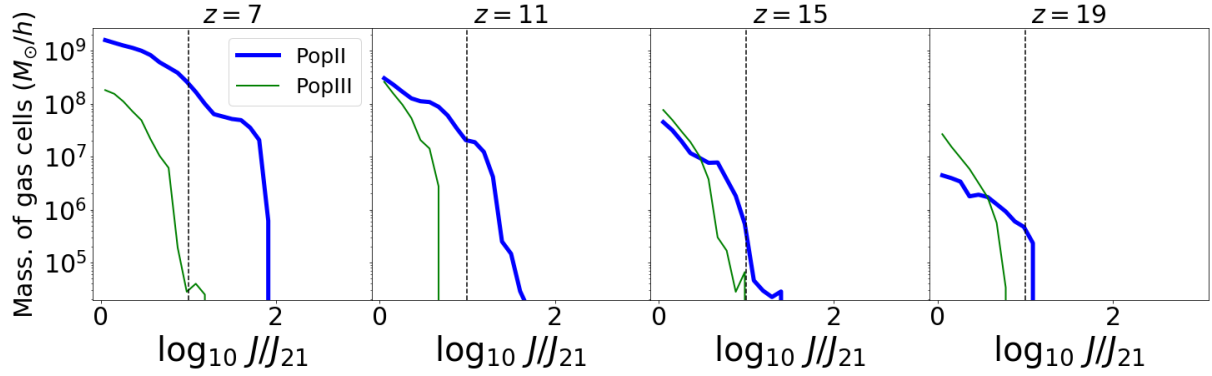


**Figure 3.** Total mass of gas cells illuminated by LW photons within bins of various flux values shown in the x-axis. Black vertical lines correspond to flux thresholds of  $J_{LW}^{\min} = 10 J_{21}$ . We find that at these flux thresholds (most relevant for BH seeding), the contribution from Pop II stars is dominant.

fore H16 can probe LW fluxes of  $300 J_{21}$  much more robustly compared to us (although at significantly lower resolutions). Additionally, there are differences in the seeding criteria applied in the two models. For example, our models apply a halo mass threshold for seeding, which is not the case for H16. Recall that in our models, seeding in lower mass halos is more strongly impacted by LW flux. Therefore, decreasing or removing the halo mass threshold would lead to a stronger impact of LW flux in our models, thereby reducing the difference between our results and those of H16. Incidentally, our results are in better agreement with the hydrodynamic simulations of Dunn et al. (2018), who find that the number of seeds is suppressed by factors of  $\sim 7$  when the critical LW flux is increased from 30 to  $300 J_{21}$ . Semi-analytic models (Agarwal et al. 2012, 2014; Dijkstra et al. 2014) exhibit an even stronger impact than that of H16, with factors of  $\sim 10^4$  decrease in the number density of DCBH forming halos when LW flux is increased from 30 to  $300 J_{21}$  (see Figure 4 of H16). As demonstrated in H16, the differences in predictions between hydrodynamic simulations and semi-analytic models may be attributed to differences in the modelling of star formation, metal enrichment, and LW radiation. Despite these differences, all the models (including this work) commonly predict a strong impact of LW radiation on black hole seeding.

The impact of the LW flux criterion versus the gas spin criterion on BH seeding can be summarized as follows. First, the LW flux criterion is overall substantially more restrictive than the gas spin criterion, particularly for lower seed masses ( $1.25 \times 10^4$  and  $1 \times 10^5 M_{\odot}/h$ , corresponding to lower halo and gas mass thresholds). Second, the LW flux criterion has a disproportionately stronger suppression for lower mass seeds and correspondingly lower mass halos, whereas the impact of the gas spin criterion is broadly similar for all seed masses. Finally, the LW flux criterion impacts seeding at all redshifts between  $z \sim 7 - 25$ , but the gas spin criterion does not significantly impact seeding at  $z \gtrsim 20$ .

When both the gas spin and LW flux criteria are applied and compared against the baseline model (blue dashed line vs black solid line in Figure 5), the number of seeds is suppressed by factors of  $\sim 300$ ,  $\sim 80$  and  $\sim 4$  for  $1.25 \times 10^4$ ,  $1 \times 10^5$  and  $8 \times 10^5 M_{\odot}/h$  seeds respectively.

### 3.4 Varying SMBH seed masses

We finally look at the implications of the foregoing results on the predictions of merger rates, BH masses, and luminosities of  $z > 7$  BHs at different seed masses (forming in halos with different total masses and star forming, metal poor gas masses).

Figure 6 shows the number of seeds born in halos of different masses. When only the baseline criteria (upper left panel of Figure 6) are applied, lower mass seeds ( $M_{\text{seed}} = 1.25 \times 10^4 M_{\odot}/h$ ) form in significantly higher numbers (by factors of  $\sim 100$ ) compared to higher mass seeds ( $M_{\text{seed}} = 8 \times 10^5 M_{\odot}/h$ ); this is because in the baseline model, lower mass seeds form in lower mass halos by construction. This continues to be true even when the gas spin criterion is added (upper right panel of Figure 6). However, when the LW flux criterion is added, seeding inside  $\lesssim 10^9 M_{\odot}$  halos is strongly suppressed (lower panels of Figure 6), which leads to disproportionately stronger suppression of lower mass seeds compared to higher mass seeds. That being said, lower mass seeds are still more abundant compared to higher mass seeds, albeit by a much smaller amount compared to when the LW flux criterion is absent.

The above trends are reflected in the BH merger rates for different seed masses shown in Figure 7. In the presence of only the baseline criteria and gas spin criterion (upper panels of Figure 7), merger rates of  $1.25 \times 10^4 M_{\odot}/h$  seeds are  $\sim 100$  times higher compared to  $8 \times 10^5 M_{\odot}/h$  seeds. But when the LW flux criterion is added (lower panels of Figure 7), merger rates of  $1.25 \times 10^4 M_{\odot}/h$  seeds are disproportionately suppressed; however, they are still slightly higher than  $1 \times 10^5 M_{\odot}/h$  seeds (by factors of  $1.5 - 2$ ). Additionally, the LW flux criterion causes the merger rates to be very low overall; there are only a handful of  $z \gtrsim 7$  mergers for  $1.25 \times 10^4$  &  $1 \times 10^5 M_{\odot}/h$  seeds, and no mergers amongst  $8 \times 10^5 M_{\odot}/h$  seeds. This indicates that if DCBHs indeed require sufficiently high LW fluxes ( $\gtrsim 10 J_{21}$ ) to form, mergers of DCBHs would be rare and challenging for LISA to detect. Lastly, note that at these redshifts, mergers are the primary channel for BH growth in our models (see Bhowmick et al. 2021 or more details); this is largely because the accretion rate scales as  $M_{bh}^2$ , which makes it difficult for low mass BHs to accrete rapidly enough. Therefore, the merger rates dominate the resulting final BH masses produced by the different seeds.



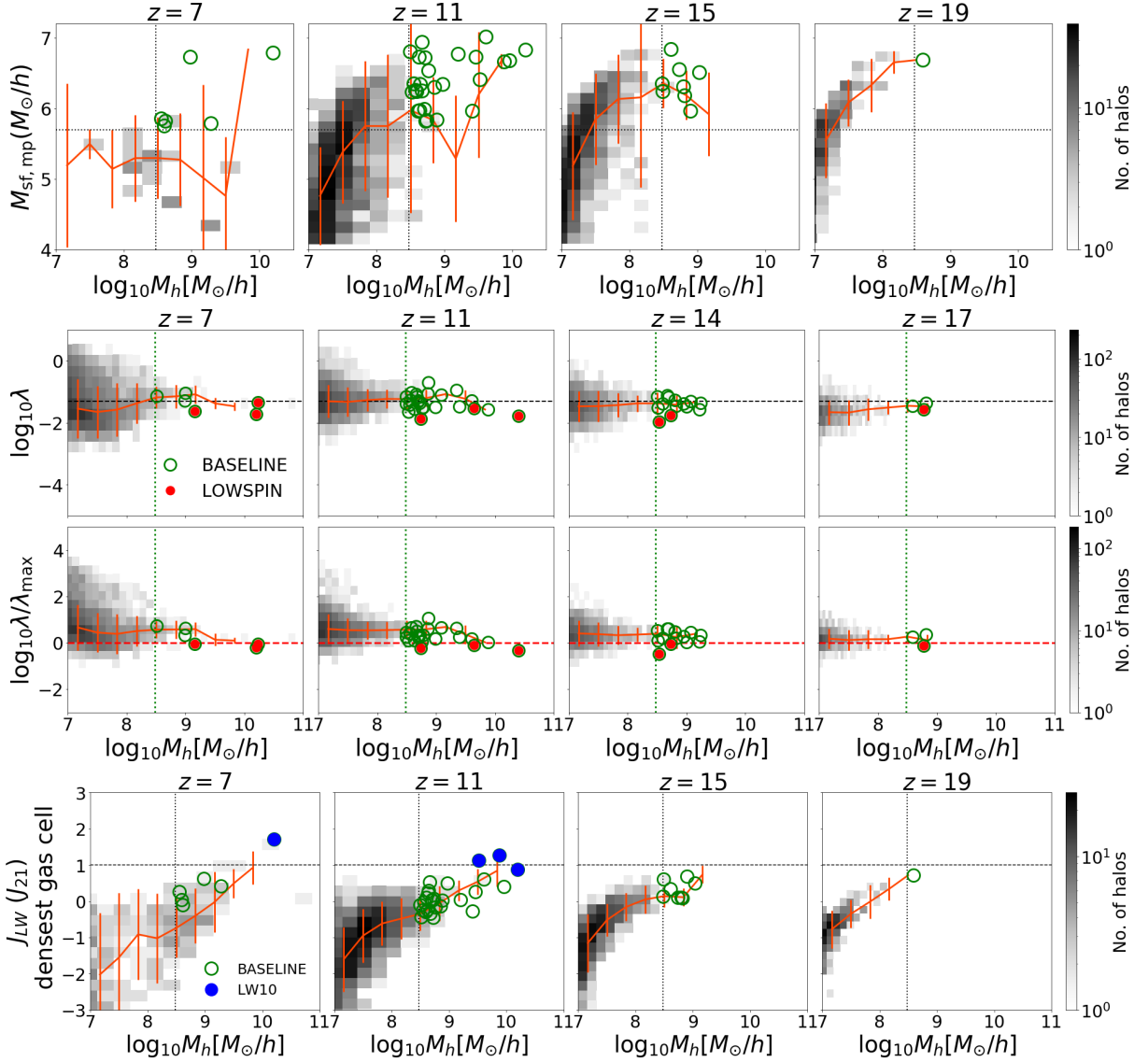


**Figure 4.** The relationships between the various halo properties that determine the formation of DCBHs at different redshifts from  $z = 7$  to  $z = 19$ . We show only halos that have  $< 1\%$  contamination from low resolution dark matter particles. The 1st row shows halo mass vs. star forming, metal poor gas mass. The 2nd row shows the halo mass ( $M_h$ ) vs. dimensionless gas spin ( $\lambda$ ). In the 3rd row, the dimensionless spins from the 2nd row are normalized with respect to the maximum value ( $\lambda_{\max}$ ) allowed for seeding to occur. The 4th row shows the halo mass vs. LW flux at the densest gas cell. The vertical lines are the minimum halo mass for seeding ( $\tilde{M}_h = 3000$ ). The horizontal line in the 1st row is the minimum star forming, metal poor gas mass for seeding ( $\tilde{M}_{\text{sf,mp}} = 5$ ). In the 3rd row, the horizontal line is the maximum gas spin ( $\lambda_{\max}$ ) that is allowed for seeding. In the 4th row, the horizontal line corresponds to  $J_{\text{LW}} = 10 J_{21}$ . Green open circles are halos that satisfy the baseline seeding criteria ( $\tilde{M}_h = 3000$ ,  $\tilde{M}_{\text{sf,mp}} = 5$ ). The red filled circles are halos that satisfy the baseline criteria as well as the gas spin criterion ( $\lambda < \lambda_{\max}$ ). The blue filled circles are halos that satisfy the baseline criteria as well as the LW flux criterion ( $M_{\text{LW}} > M_{\text{seed}}$ ;  $J_{\text{LW}}^{\text{min}} = 10 J_{21}$ ). We find that a small fraction of halos which satisfy the baseline seeding criteria also satisfy the gas spin and LW flux criterion.

The final BH masses at  $z = 7, 11, 14$  produced by  $1.25 \times 10^4$ ,  $1 \times 10^5$  &  $8 \times 10^5 M_{\odot}/h$  seeds are shown in Figure 8 for our models with different combinations of baseline seeding criteria, gas spin criterion, and LW flux criterion. When only the baseline seeding criteria are applied (1st row of Figure 8), we find that seed masses of  $1.25 \times 10^4$ ,  $1 \times 10^5$  &  $8 \times 10^5 M_{\odot}/h$  produce similar black hole mass (at fixed halo mass) for  $z \sim 7 - 11$ , reiterating the results from Bhowmick et al. (2021). This continues to be true when the gas spin criteria are added (2nd row of Figure 8), and directly follows from

the results of Figures 6 and 7. More specifically, since lower mass seeds form in lower mass halos, the earlier formation times and higher merger rates allow them to grow and reach similar masses as that of higher mass seeds that form at later times (in higher mass halos). When the LW flux is added (3rd and 4th rows of Figure 8), the results are dramatically different. Firstly, BHs primarily occupy halos  $\gtrsim 10^9 M_{\odot}/h$  as a natural consequence of the strong suppression of seed formation in lower mass halos. Due to the resulting disproportionate suppression of lower mass seeds, they can no longer

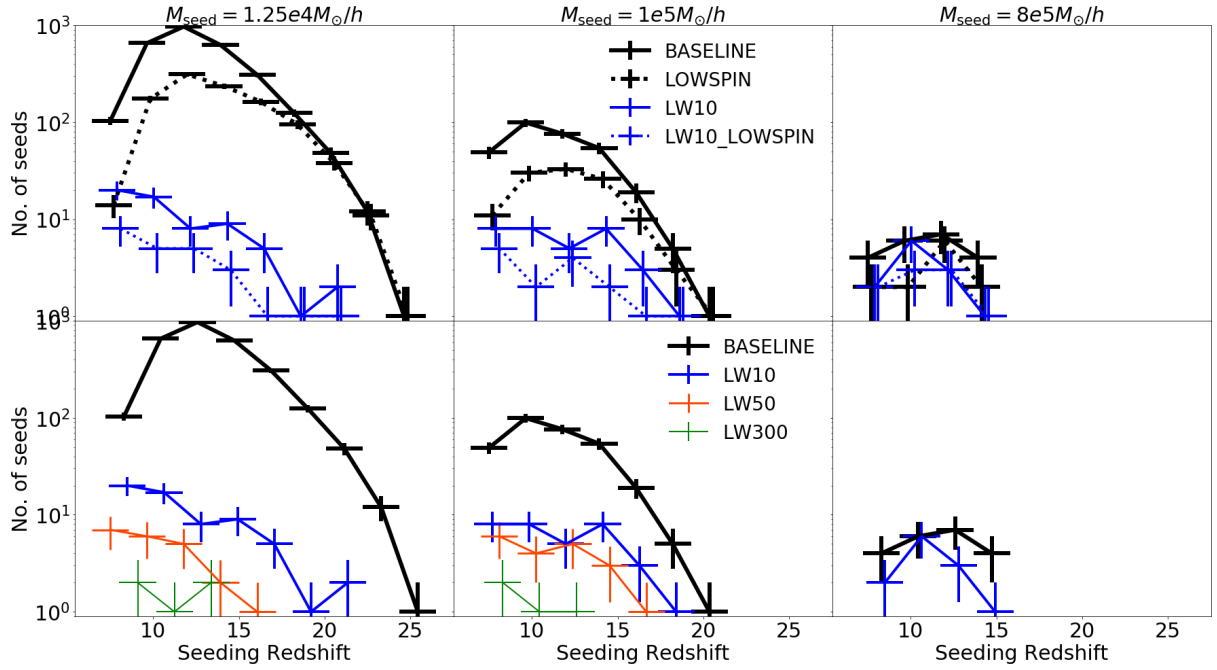


**Figure 5.** Distribution of seeding times for different seed models at fixed  $M_{\text{seed}}$ . Dashed vs solid lines (of the same color) in the upper panels correspond to models with vs. without the gas spin criterion, respectively. The suppression due to the gas spin criterion is by factors of  $\sim 6$  for all seed masses at  $z \sim 11 - 12$  (when most seeds form). Colored vs. black lines in the lower panels compare models with vs. without a LW flux criterion respectively. When  $J_{21}^{\text{min}} = 10 J_{21}$  is applied, the number of seeds is suppressed up to factors of  $\sim 100$ ,  $\sim 10$  and  $\sim 3$  for  $M_{\text{seed}} = 1.25 \times 10^4$ ,  $1 \times 10^5$  and  $8 \times 10^5 M_{\odot}/h$  respectively.

merge fast enough to produce similar BH masses (at fixed halo mass) to that of higher mass seeds; BHs formed from  $1.25 \times 10^4 M_{\odot}/h$  seeds are  $\sim 100$  times less massive compared to those formed from  $8 \times 10^5 M_{\odot}/h$  seeds. In fact, neither  $1.25 \times 10^4 M_{\odot}/h$  nor  $1 \times 10^5 M_{\odot}/h$  seeds are able to form SMBHs of masses  $\gtrsim 10^6 M_{\odot}/h$  by  $z = 7$  in our simulation volume.

Lastly, we look at the BH luminosities produced by  $1.25 \times 10^4$ ,  $1 \times 10^5$  &  $8 \times 10^5 M_{\odot}/h$  seeds (color coded in the data points of Figure 8). These luminosities were estimated from the BH accretion rates using Eq. (4). For models with only the baseline seeding criteria and gas spin criteria, the different seed masses produce similar BH luminosities at fixed halo mass. When the LW flux criterion is added,  $1.25 \times 10^4 M_{\odot}/h$  seeds produce  $\sim 1000$  times fainter luminosities at  $z \sim 7 - 11$ , compared to  $8 \times 10^5 M_{\odot}/h$  seeds; this is not unexpected given the differences in the final BH masses produced by  $1.25 \times 10^4$  vs.  $8 \times 10^5 M_{\odot}/h$  seeds. We also compare these luminosities to the Lynx 2 – 10 keV band detection limit of  $1 \times 10^{-19} \text{ ergs cm}^{-2} \text{ s}^{-1}$  (marked in the color-bar of Figure 8 for  $z = 7, 11, 14$ ). The assumed bolometric correction is adopted from Vasudevan & Fabian (2007). We first note that AGN above this detection limit (highlighted red data points in Figure 8) are overall rare in our zoom volumes. For the very few AGN that do exceed this detection limit, we find that in the presence of LW flux criterion, they can only be produced by the most massive  $8 \times 10^5 M_{\odot}/h$  seeds. We note that these luminosities are subject to theoretical uncertainties in our BH accretion model as well as the bolometric corrections.

Overall, these results imply that DCBH formation sites occur predominantly in halos  $\gtrsim 10^9 M_{\odot}/h$ , which typically

begin assembling in significant numbers after  $z \sim 16$ . Seeds forming within these halos must already have high enough initial seed masses (a few  $\times 10^5 M_{\odot}/h$  or higher) to produce BHs in the supermassive regime ( $\gtrsim 10^6 M_{\odot}/h$ ) by  $z \sim 7$ . We again emphasize that the foregoing implications are very specific to our underlying assumption of Bondi accretion, which struggles to grow low mass BHs at early times due to the  $\sim M_{bh}^2$  scaling of the accretion rate. Additionally, even if the Bondi accretion model is accurate, our conclusions do not necessarily apply to the regime of the observed  $z \gtrsim 7$  quasars with BH masses up to  $\sim 10^9 M_{\odot}/h$ . This is because high- $z$  quasars are expected to reside in much more extreme regions than our zoom volume, where accretion will have a more significant (and potentially dominant) contribution. This means that our conclusions may change when our models are applied to these extreme regions, and do not yet rule out the possibility of lower mass ( $\sim 10^4 M_{\odot}/h$ ) DCBH seeds as progenitors of  $z \gtrsim 7$  quasars; we shall explore this in future work.

#### 4 SUMMARY AND CONCLUSIONS

In this work, we explore seeding conditions typically associated with DCBH seed formation, and assess their influence on the  $z \gtrsim 7$  SMBH populations using cosmological hydrodynamical simulations. In particular, we quantify the impact of restricting seeds to halos with low gas spins, and exposed to LW radiation.

We start with a set of baseline seeding criteria as outlined in Bhowmick et al. (2021) to ensure that seeds are formed only in pristine star forming halos: BH seeding sites are required to have a minimum threshold of total halo mass ( $3000 M_{\text{seed}}$ )

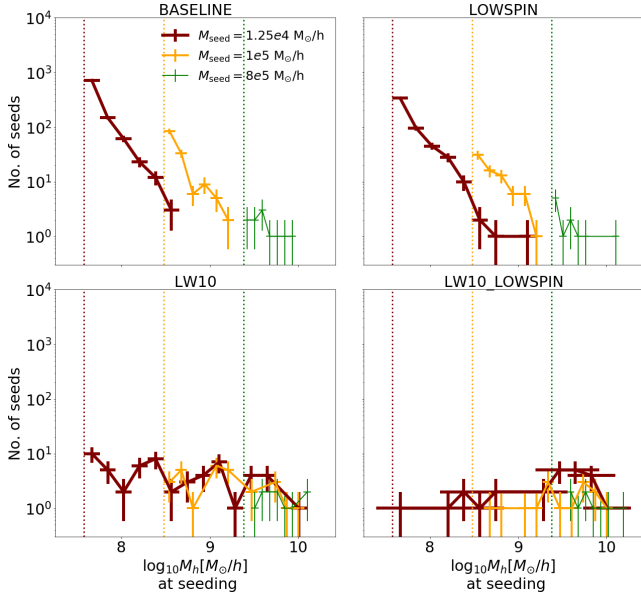


**Figure 6.** Number of seeding events in various bins of host halo masses for models with  $M_{\text{seed}} = 1.25 \times 10^4$ ,  $1 \times 10^5$ ,  $8 \times 10^5 M_{\odot}/h$ . The vertical dotted lines show the minimum halo mass for seeding ( $\tilde{M}_h \times M_{\text{seed}}$ ). In the upper left panel, we apply only the baseline criteria for halo mass ( $\tilde{M}_h = 3000$ ) and star forming, metal poor gas mass ( $\tilde{M}_{\text{sf,mp}} = 5$ ). In the upper right panel, we additionally apply the gas spin criterion. In the lower left panel, we additionally apply the LW flux criterion ( $J_{\text{LW}}^{\text{min}} = 10 J_{21}$ ). Lastly, the lower right panels apply both the gas spin and LW flux criteria. When only the baseline criteria and gas spin criterion are applied, the number of  $1.25 \times 10^4 M_{\odot}/h$  seeds is up to  $\sim 10$  ( $\sim 100$ ) times higher than  $1 \times 10^5 M_{\odot}/h$  ( $8 \times 10^5 M_{\odot}/h$ ) seeds; this is because lower seed masses are able to form in lower mass halos, which are more abundant. When the LW flux criterion is added, the seeding is strongly suppressed in lower mass halos ( $\lesssim 10^9 M_{\odot}$ ).

and star forming, metal poor gas mass ( $5 M_{\text{seed}}$ ). We then add the gas spin and LW flux criteria, and focus on their impact on seed formation and the resulting  $z \gtrsim 7$  SMBH populations. These are described as:

- *Gas spin criterion:* The dimensionless spin angular momentum ( $\lambda$ ) of the gas in the host halo must be less than the minimum value ( $\lambda_{\text{max}}$ ) required for the gas disc to be gravitationally stable.
- *LW flux criterion:* Halos must have a minimum mass of gas (greater than or equal to the seed mass  $M_{\text{seed}}$ ) that is exposed to LW fluxes greater than a critical threshold  $J_{\text{LW}}^{\text{min}}$ , in order to inhibit gas fragmentation via  $\text{H}_2$  cooling.

We explored  $M_{\text{seed}}$  values of  $1.25 \times 10^4$ ,  $1 \times 10^5$  and  $8 \times 10^5 M_{\odot}/h$ , which broadly cover the range of DCBH seed masses inferred from theoretical models.

Our key findings are as follows:

- When seeding is limited to halos with low gas spin ( $\lambda < \lambda_{\text{max}}$ ), the overall rates of seed formation are suppressed by factors of  $\sim 6$  for all seed masses, particularly at  $z \sim 11 - 12$  when most seeds form. The gas spin criterion has a weaker effect at higher redshifts and is negligible at  $z \gtrsim 20$ .
- BH seeding is strongly suppressed in  $\lesssim 10^9 M_{\odot}/h$  halos when a minimum incident LW flux criterion is added to the baseline seed model. This disproportionately sup-

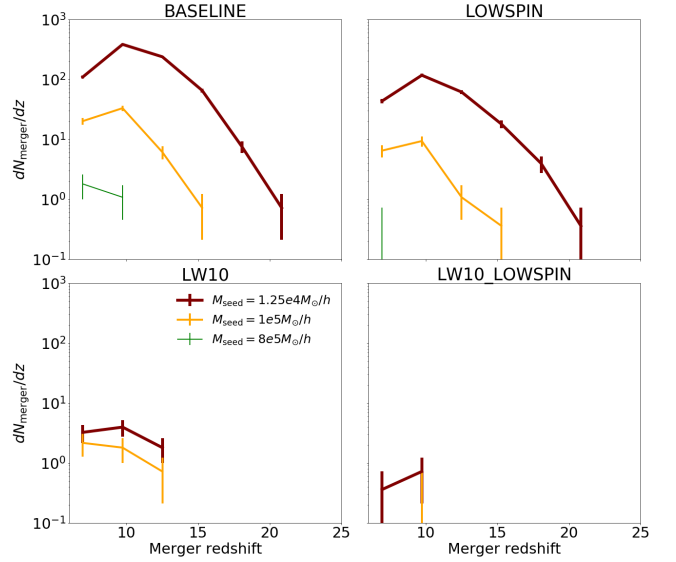


**Figure 7.** Same as previous figure, but for the merger rates. When the baseline criterion and gas spin criterion are applied,  $1.25 \times 10^4 M_{\odot}/h$  seeds merge  $\sim 10$  ( $\sim 100$ ) times more frequently than  $1 \times 10^5 M_{\odot}/h$  ( $8 \times 10^5 M_{\odot}/h$ ) seeds. But when the LW flux criterion is applied, the merger rate for  $1.25 \times 10^4 M_{\odot}/h$  seeds is disproportionately suppressed; despite this, it is still slightly higher (factors of  $1.5 - 2$ ) compared to  $1 \times 10^5 M_{\odot}/h$  seeds. Additionally, there are no merger events amongst  $8 \times 10^5 M_{\odot}/h$  seeds in the presence of the LW flux criterion.

presses lower mass seeds ( $1.25 \times 10^4 M_{\odot}/h$ ) compared to the baseline model (which otherwise forms lower mass seeds in correspondingly lower mass halos). The formation of  $1.25 \times 10^4 M_{\odot}/h$  seeds is suppressed by factors of  $\sim 100$  for  $J_{\text{LW}}^{\text{min}} > 10 J_{21}$ . In contrast, the formation of the most massive  $8 \times 10^5 M_{\odot}/h$  seeds is suppressed by factors of  $\sim 3$ , as these seeds are already restricted to formation in more massive halos. Despite the disproportionate suppression, the number of lower mass seeds formed is still greater than the number of higher mass seeds.

(iii) When both the gas-spin and LW flux criteria ( $J_{\text{LW}}^{\text{min}} = 10 J_{21}$ ) are imposed (in addition to the baseline model), seed formation is even more strongly suppressed. Relative to the baseline model, seeding events are suppressed by factors of  $\sim 300$ ,  $\sim 80$  and  $\sim 4$  for seed masses of  $1.25 \times 10^4$ ,  $1 \times 10^5$  and  $8 \times 10^5 M_{\odot}/h$  respectively.

(iv) Merger rates of  $1.25 \times 10^4 M_{\odot}/h$  seeds are  $\sim 10$  ( $\sim 100$ ) times higher than  $1 \times 10^5 M_{\odot}/h$  ( $8 \times 10^5 M_{\odot}/h$ ) seeds when seeding is only limited by the gas spin criterion and not limited by a LW flux criterion. This occurs because lower mass seeds form in lower mass halos, which are more numerous. When the seeds are limited to halos with LW fluxes  $\gtrsim 10 J_{21}$ , merger rates of lower mass seeds are disproportionately suppressed since they can no longer form in  $\lesssim 10^9 M_{\odot}/h$  halos. This also causes the merger rates to be very low overall, with only a handful of mergers for  $1.25 \times 10^4$  &  $1 \times 10^5 M_{\odot}/h$  seeds and none for  $8 \times 10^5 M_{\odot}/h$  seeds.

(v) With the addition of a LW flux criterion,  $8 \times 10^5 M_{\odot}/h$  seeds produce BHs at  $z \sim 7 - 11$  that are generally  $\sim 1000$  times more luminous and  $\sim 50$  times more massive, compared to that of  $1.25 \times 10^4 M_{\odot}/h$  seeds. This arises due to the disproportionately strong suppression in merger rates for

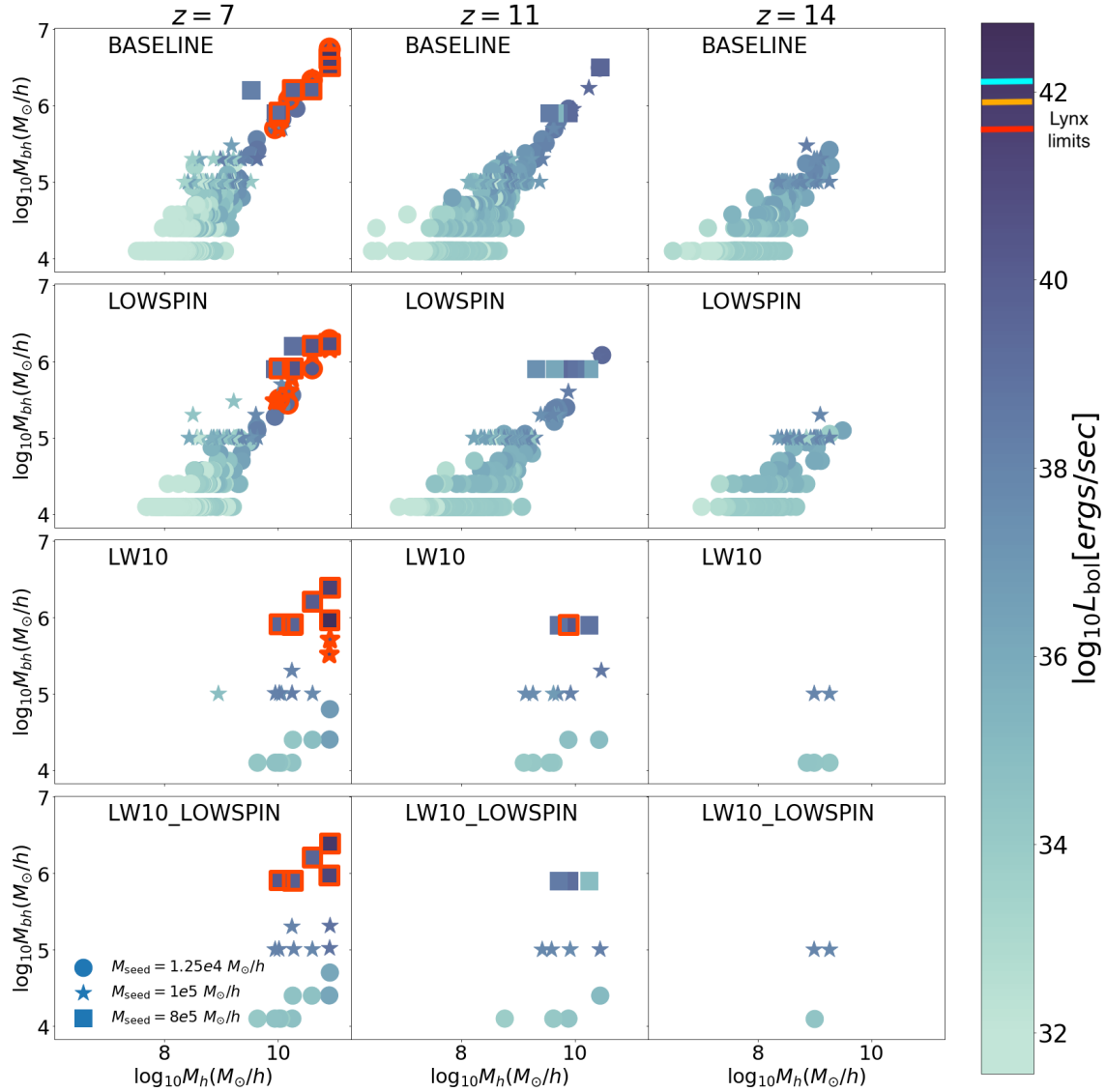


**Figure 8.** Halo mass vs total black hole mass relation for  $M_{\text{seed}} = 1.25 \times 10^4, 1 \times 10^5, 8 \times 10^5 M_{\odot}/h$ . The data points are color coded by the black hole luminosity. Only those halos are shown where  $< 1\%$  of the total mass is contaminated by low resolution DM particles. Left to right panels correspond to different redshift snapshots. In the 1st row, we only apply the baseline criteria for halo mass ( $\tilde{M}_h = 3000$ ) and star forming, metal poor gas mass ( $\tilde{M}_{\text{sf,mp}} = 5$ ). In the 2nd row, we additionally apply the gas spin criterion. In the 3rd row, we additionally apply the LW flux criterion ( $J_{\text{LW}}^{\text{min}} = 10 J_{21}$ ). In the 4th row, we apply both the gas spin and LW flux criteria. The red, orange and cyan markers on the color bar correspond to the detection limit of Lynx at  $z = 7, 11, 14$  respectively; this is assumed to be  $1 \times 10^{-19} \text{ ergs cm}^{-2} \text{ s}^{-1}$  in the 2–10 keV band for a survey area of 360 arcmin<sup>2</sup> (Griffin et al. 2020). The required bolometric correction is adopted from Vasudevan & Fabian (2007). The points that are highlighted in red correspond to objects which surpass the Lynx detection limit. When the baseline and gas spin criteria are applied, different seed masses produce BHs with similar masses and luminosities at fixed halo mass. This is because lower mass seeds form in lower mass halos that assemble earlier; as a result, they merge and grow more rapidly compared to the higher mass seeds that form later. The foregoing is no longer true when the LW flux criterion is applied because seeding is strongly suppressed in  $\lesssim 10^9 M_{\odot}/h$  halos. As a result, at fixed halo mass,  $1.25 \times 10^4 M_{\odot}/h$  seeds produce BHs that are  $\sim 50$  times less massive and  $\sim 1000$  times less luminous compared to  $8 \times 10^5 M_{\odot}/h$  seeds at  $z \sim 7 - 11$ .

lower mass seeds. In fact, only the  $8 \times 10^5 M_{\odot}/h$  seeds are able to form BHs in the supermassive regime ( $\gtrsim 10^6 M_{\odot}/h$ ) at  $z \sim 7 - 11$  in our simulations. This is in stark contrast to models with only the baseline seeding criteria and gas spin criterion, wherein all the seed masses form SMBHs up to similar masses ( $\sim 5 \times 10^6 - 10^7 M_{\odot}/h$ ) and luminosities ( $\sim 10^{42} - 10^{43} \text{ ergs/sec}$ ) at  $z \sim 7 - 11$ .

Overall, we find that both the gas spin and LW flux cri-

teria significantly impact BH seed formation. The LW flux criterion tends to have a much stronger impact, particularly for low mass seeds ( $\sim 10^4 M_{\odot}/h$ ) forming in lower mass halos. Because the early growth histories of BHs are merger-dominated in our simulations, the drastic suppression of seed formation in  $\lesssim 10^9 M_{\odot}/h$  halos make it difficult for lower mass seeds to grow to the supermassive regime by  $z \sim 7$ . At the other end, very massive seeds (a few times  $\sim 10^5 M_{\odot}/h$ )



do have a better chance at producing SMBHs, but it is unclear how abundantly they form over much larger cosmological volumes. Our findings agree with the general consensus that conditions for DCBH seed formation are very restrictive (Dijkstra et al. 2014; Habouzit et al. 2016). Without a more significant contribution to BH growth from gas accretion, it would be challenging to explain a sizable majority of  $z > 7$  SMBHs solely using DCBH channels.

Our results are quantitatively consistent with some of the previous works, but have differences compared to others. For instance, the impact of gas spin predicted by our model is similar to that of Lodato & Natarajan (2006). In terms of LW flux criterion, we predict a similar impact as the hydrodynamic simulations of Dunn et al. (2018), but a somewhat smaller impact compared to H16. Note however that due to a relatively small zoom volume, our results are not as statistically robust for the highest fluxes ( $\gtrsim 300 J_{21}$ ) compared to the largest volume of H16 (142 Mpc/h per side). Semi-analytic models (Agarwal et al. 2012, 2014; Dijkstra et al. 2014) predict a substantially stronger impact (by factors  $\gtrsim 100$ ) of LW flux compared to hydrodynamic simulations; this can be attributed to differences in the modelling of star formation, metal enrichment, and LW radiation (as demonstrated by H16). Regardless of the quantitative differences, all of these works agree that both gas spin and LW flux can have a substantial impact on seed formation. Our work additionally demonstrates that the LW flux criterion tends to be more restrictive compared to the gas spin criterion. Our results have several potential implications for upcoming observational facilities. The fact that the LW flux criterion strongly restricts seeding below  $\lesssim 10^9 M_\odot/h$  halos has two important observational consequences. First, the resulting merger rates are very low, implying that LISA may find it much more challenging to detect mergers originating from DCBH channels, compared to other channels (e.g. Pop III). Second, for the events that are detected by LISA, follow-up electromagnetic observations of their host galaxies using JWST may be useful for constraining their seeding origins. Electromagnetic observations may also be able to distinguish other signatures of the DCBH seeding models presented here.

In Bhowmick et al. (2021), we found that for our baseline seed model, it would be difficult for surveys like Lynx or JWST to distinguish between the AGN luminosity function predictions for different seeding criteria. This is no longer true when the LW flux criterion is applied, which substantially modifies the BH luminosities produced by different seed masses. However, note that our zoom volume produces very few objects that would be detectable with Lynx. Simulations of larger volumes will be required to constrain the high-redshift AGN luminosity function resulting from our seed models, which we will explore in future work. Overall, our results suggest that if DCBHs indeed form only in the presence of sufficiently high LW fluxes ( $\gtrsim 10 J_{21}$ ), future observational facilities may be able to distinguish between seeds formed from DCBH channels vs. other channels; this is in broad agreement with previous works (Agarwal et al. 2013; Natarajan et al. 2017; Visbal & Haiman 2018).

Our results are strongly influenced by the fact that at these early epochs, BH growth is dominated by BH mergers, and there is very little growth due to gas accretion. This is a well-known issue in simulating the growth of low-mass BH seeds, which owes in large part to the  $M_{\text{BH}}^2$  scaling of the

Bondi-Hoyle accretion model. A variety of alternate accretion models exist in the literature (Pelupessy et al. 2007; Booth & Schaye 2009; Tremmel et al. 2017; Zhu et al. 2020), but the  $M_{\text{BH}}^2$  scaling is generic to all models in which the gas capture radius is assumed to scale with BH mass.

Alternate accretion models exist that can have much smaller scaling exponents for the accretion rate vs. BH mass (e.g.  $\propto M_{\text{bh}}^{1/6}$  for accretion driven by stellar gravitational torques (Hopkins & Quataert 2011; Anglés-Alcázar et al. 2017; Davé et al. 2019)). If such a model can be reliably applied in the high-redshift regime, this might significantly boost early growth. Additionally, we note that both accretion rates and merger rates are likely to be influenced by the BH repositioning scheme, which causes the BHs to rapidly sink to the halo centers. Recent work incorporating more realistic subgrid prescriptions for modeling unresolved dynamical friction has been shown to increase merger times and decrease accretion rates (Tremmel et al. 2017; Bellovary et al. 2021). We plan to explore the impact of BH dynamics on early seed growth in future work.

Finally, we emphasize that the results of this work should not be extrapolated to the regime of observed high redshift quasars, since they are likely a tiny fraction of the overall SMBH population forming in regions much more overdense than our zoom volume. In such extreme regions, we can expect gas accretion to have an increasingly significant (and potentially dominant) role in the BH growth.

Lastly, while this work focuses on the DCBH channel, it is part of a continued series of studies on the underlying seeding prescriptions, agnostic about the physical channels they may represent. Between this work and Bhowmick et al. (2021), we have now expanded our seeding models to encompass most of the physical properties commonly associated with theoretical gas-dependent BH seed formation channels. These works will serve as a basis for continued development of seeding prescriptions, particularly in the context of large volume uniform simulations.

## APPENDIX A: RESOLUTION CONVERGENCE

Here, we look at the resolution convergence of our gas based seed models. In Bhowmick et al. (2021), we demonstrated that our baseline models were reasonably well converged for  $L_{\text{max}} \geq 11$ . It is instructive to check whether this resolution convergence is retained even after applying the gas spin and LW flux criteria. Figure A1 compares the number of seeds formed by our gas based seed models at resolutions of  $L_{\text{max}} = 10, 11, 12$ . We find that in the presence of gas spin (1st panel) as well as LW flux criterion (2nd, 3rd and 4th panels), the differences between  $L_{\text{max}} = 12$  vs. 11 are smaller than the differences between  $L_{\text{max}} = 11$  vs. 10. This indicates that our models exhibit resolution convergence. By  $L_{\text{max}} = 11$ , the number of seeds are reasonably well converged (to within factors of  $\sim 1.7$ ). Therefore, we choose  $L_{\text{max}} = 11$  for analyzing our data as it provides sufficiently accurate results at reasonable computational expense.

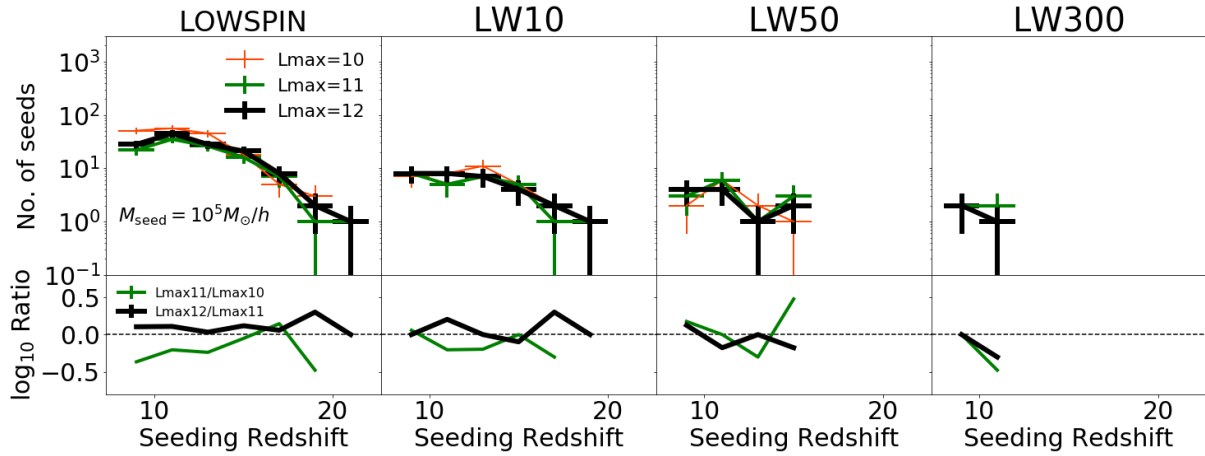


**Figure A1.** Resolution convergence of the distribution of seeding times for  $M_{\text{seed}} = 10^5 M_{\odot}/h$ ,  $\tilde{M}_h = 3000$  &  $\tilde{M}_{\text{sf,mp}} = 5$ . Red, green and black lines in the upper panels correspond to  $L_{\text{max}} = 10, 11$  &  $12$  respectively. The 1st panel corresponds to the baseline + gas spin criterion; 2nd, 3rd and 4th panels correspond to baseline + Lyman Werner flux criterion for  $J_{\text{LW}}^{\text{min}} = 10, 50$  &  $300 J_{21}$ . Green and black lines in the lower panels show the ratios between  $L_{\text{max}} = 11$  vs.  $10$  and  $L_{\text{max}} = 12$  vs.  $11$  respectively. Across all the models, we can see that the difference in predictions between successive values of  $L_{\text{max}}$  decreases with increasing resolution. This indicates that our model predictions show resolution convergence.

## ACKNOWLEDGEMENTS

LB acknowledges support from National Science Foundation grant AST-1715413. LB and PT acknowledges support from NSF grant AST-1909933 and NASA ATP Grant 80NSSC20K0502. PT also acknowledges support from AST-200849. DN acknowledges funding from the Deutsche Forschungsgemeinschaft (DFG) through an Emmy Noether Research Group (grant number NE 2441/1-1). MV acknowledges support through NASA ATP grants 16-ATP16-0167, 19-ATP19-0019, 19-ATP19-0020, 19-ATP19-0167, and NSF grants AST-1814053, AST-1814259, AST-1909831 and AST-2007355.

## DATA AVAILABILITY

The underlying data used in this work shall be made available upon reasonable request to the corresponding author.

## REFERENCES

Agarwal B., Khochfar S., Johnson J. L., Neistein E., Dalla Vecchia C., Livio M., 2012, *MNRAS*, **425**, 2854  
 Agarwal B., Davis A. J., Khochfar S., Natarajan P., Dunlop J. S., 2013, *MNRAS*, **432**, 3438  
 Agarwal B., Dalla Vecchia C., Johnson J. L., Khochfar S., Paardekooper J.-P., 2014, *MNRAS*, **443**, 648  
 Anglés-Alcázar D., Davé R., Faucher-Giguère C.-A., Özel F., Hopkins P. F., 2017, *MNRAS*, **464**, 2840  
 Bañados E., et al., 2018, *Nature*, **553**, 473  
 Baker J., et al., 2019, arXiv e-prints, p. [arXiv:1907.06482](https://arxiv.org/abs/1907.06482)  
 Barnes J., Hut P., 1986, *Nature*, **324**, 446  
 Becerra F., Marinacci F., Bromm V., Hernquist L. E., 2018, *MNRAS*, **480**, 5029  
 Begelman M. C., 2010, *MNRAS*, **402**, 673  
 Begelman M. C., Volonteri M., Rees M. J., 2006, *MNRAS*, **370**, 289  
 Bellovary J. M., et al., 2021, arXiv e-prints, p. [arXiv:2102.09566](https://arxiv.org/abs/2102.09566)

Bett P., Eke V., Frenk C. S., Jenkins A., Helly J., Navarro J., 2007, *MNRAS*, **376**, 215  
 Bett P., Eke V., Frenk C. S., Jenkins A., Okamoto T., 2010, *MNRAS*, **404**, 1137  
 Bhowmick A. K., et al., 2021, arXiv e-prints, p. [arXiv:2105.08055](https://arxiv.org/abs/2105.08055)  
 Booth C. M., Schaye J., 2009, *MNRAS*, **398**, 53  
 Bromm V., Loeb A., 2003, *ApJ*, **596**, 34  
 Bullock J. S., Dekel A., Kolatt T. S., Kravtsov A. V., Klypin A. A., Porciani C., Primack J. R., 2001, *ApJ*, **555**, 240  
 Chabrier G., 2003, *PASP*, **115**, 763  
 Chon S., Hosokawa T., Omukai K., 2021, *MNRAS*, **502**, 700  
 Danovich M., Dekel A., Hahn O., Ceverino D., Primack J., 2015, *MNRAS*, **449**, 2087  
 Davé R., Anglés-Alcázar D., Narayanan D., Li Q., Rafieferantsoa M. H., Appleby S., 2019, *MNRAS*, **486**, 2827  
 DeGraf C., Sijacki D., 2020, *MNRAS*, **491**, 4973  
 Dijkstra M., Haiman Z., Mesinger A., Wyithe J. S. B., 2008, *MNRAS*, **391**, 1961  
 Dijkstra M., Ferrara A., Mesinger A., 2014, *MNRAS*, **442**, 2036  
 Dunn G., Bellovary J., Holley-Bockelmann K., Christensen C., Quinn T., 2018, *ApJ*, **861**, 39  
 Fan X., et al., 2001, *AJ*, **122**, 2833  
 Fryer C. L., Woosley S. E., Heger A., 2001, *ApJ*, **550**, 372  
 Gardner J. P., et al., 2006, *Space Sci. Rev.*, **123**, 485  
 Genel S., et al., 2014, *MNRAS*, **445**, 175  
 Glover S. C. O., 2015, *MNRAS*, **451**, 2082  
 Grand R. J. J., et al., 2017, *MNRAS*, **467**, 179  
 Griffin A. J., Lacey C. G., Gonzalez-Perez V., Lagos C. d. P., Baugh C. M., Fanidakis N., 2020, *MNRAS*, **492**, 2535  
 Habouzit M., Volonteri M., Latif M., Dubois Y., Peirani S., 2016, *MNRAS*, **463**, 529  
 Hahn O., Abel T., 2011, *MNRAS*, **415**, 2101  
 Harms R. J., et al., 1994, *ApJ*, **435**, L35  
 Hopkins P. F., Quataert E., 2011, *MNRAS*, **415**, 1027  
 Hosokawa T., Omukai K., Yorke H. W., 2012, *ApJ*, **756**, 93  
 Hosokawa T., Yorke H. W., Inayoshi K., Omukai K., Yoshida N., 2013, *ApJ*, **778**, 178  
 Huang K.-W., Di Matteo T., Bhowmick A. K., Feng Y., Ma C.-P., 2018, *MNRAS*, **478**, 5063  
 Johnson J. L., Dalla Vecchia C., Khochfar S., 2013, *MNRAS*, **428**, 1857  
 Kormendy J., Richstone D., 1992, *ApJ*, **393**, 559

- Koushiappas S. M., Bullock J. S., Dekel A., 2004, *MNRAS*, **354**, 292
- Latif M. A., Bovino S., Van Borm C., Grassi T., Schleicher D. R. G., Spaans M., 2014, *MNRAS*, **443**, 1979
- Latif M. A., Schleicher D. R. G., Hartwig T., 2016, *MNRAS*, **458**, 233
- Leitherer C., et al., 1999, *ApJS*, **123**, 3
- Libeskind N. I., et al., 2020, *MNRAS*, **498**, 2968
- Lodato G., Natarajan P., 2006, *MNRAS*, **371**, 1813
- Lodato G., Natarajan P., 2007, *MNRAS*, **377**, L64
- Luo Y., Ardaneh K., Shlosman I., Nagamine K., Wise J. H., Begelman M. C., 2018, *MNRAS*, **476**, 3523
- Luo Y., Shlosman I., Nagamine K., Fang T., 2020, *MNRAS*, **492**, 4917
- Macciò A. V., Dutton A. A., van den Bosch F. C., Moore B., Potter D., Stadel J., 2007, *MNRAS*, **378**, 55
- Madau P., Rees M. J., 2001, *ApJ*, **551**, L27
- Marinacci F., et al., 2018, *MNRAS*, **480**, 5113
- Miyoshi M., Moran J., Herrnstein J., Greenhill L., Nakai N., Diamond P., Inoue M., 1995, *Nature*, **373**, 127
- Mortlock D. J., et al., 2011, *Nature*, **474**, 616
- Naiman J. P., et al., 2018, *MNRAS*, **477**, 1206
- Natarajan P., Volonteri M., 2012, *MNRAS*, **422**, 2051
- Natarajan P., Pacucci F., Ferrara A., Agarwal B., Ricarte A., Zackrisson E., Cappelluti N., 2017, *ApJ*, **838**, 117
- Nelson D., et al., 2015, *Astronomy and Computing*, **13**, 12
- Nelson D., et al., 2018, *MNRAS*, **475**, 624
- Nelson D., et al., 2019a, *Computational Astrophysics and Cosmology*, **6**, 2
- Nelson D., et al., 2019b, *MNRAS*, **490**, 3234
- Omukai K., 2001, *ApJ*, **546**, 635
- Pakmor R., Bauer A., Springel V., 2011, *MNRAS*, **418**, 1392
- Pakmor R., Pfrommer C., Simpson C. M., Kannan R., Springel V., 2016, *MNRAS*, **462**, 2603
- Pelupessy F. I., Di Matteo T., Ciardi B., 2007, *ApJ*, **665**, 107
- Pillepich A., et al., 2018a, *MNRAS*, **473**, 4077
- Pillepich A., et al., 2018b, *MNRAS*, **475**, 648
- Pillepich A., et al., 2019, *MNRAS*, **490**, 3196
- Planck Collaboration et al., 2016, *A&A*, **594**, A13
- Regan J. A., Johansson P. H., Wise J. H., 2014, *ApJ*, **795**, 137
- Regan J. A., Haiman Z., Wise J. H., O'Shea B. W., Norman M. L., 2020a, *The Open Journal of Astrophysics*, **3**, E9
- Regan J. A., Wise J. H., Woods T. E., Downes T. P., O'Shea B. W., Norman M. L., 2020b, *The Open Journal of Astrophysics*, **3**, 15
- Ricarte A., Natarajan P., 2018, *MNRAS*, **481**, 3278
- Schaerer D., 2002, *A&A*, **382**, 28
- Schäfer B. M., 2009, *International Journal of Modern Physics D*, **18**, 173
- Schleicher D. R. G., Palla F., Ferrara A., Galli D., Latif M., 2013, *A&A*, **558**, A59
- Shang C., Bryan G. L., Haiman Z., 2010, *MNRAS*, **402**, 1249
- Sijacki D., Vogelsberger M., Genel S., Springel V., Torrey P., Snyder G. F., Nelson D., Hernquist L., 2015, *MNRAS*, **452**, 575
- Spergel D., et al., 2015, arXiv e-prints, p. arXiv:1503.03757
- Springel V., 2010, *MNRAS*, **401**, 791
- Springel V., Hernquist L., 2003, *MNRAS*, **339**, 289
- Springel V., et al., 2018, *MNRAS*, **475**, 676
- The Lynx Team 2018, arXiv e-prints, p. arXiv:1809.09642
- Tremmel M., Karcher M., Governato F., Volonteri M., Quinn T. R., Pontzen A., Anderson L., Bellovary J., 2017, *MNRAS*, **470**, 1121
- Vasudevan R. V., Fabian A. C., 2007, *MNRAS*, **381**, 1235
- Visbal E., Haiman Z., 2018, *ApJ*, **865**, L9
- Vogelsberger M., Genel S., Sijacki D., Torrey P., Springel V., Hernquist L., 2013, *MNRAS*, **436**, 3031
- Vogelsberger M., et al., 2014, *MNRAS*, **444**, 1518
- Vogelsberger M., Marinacci F., Torrey P., Puchwein E., 2020, *Nature Reviews Physics*, **2**, 42
- Volonteri M., Madau P., Haardt F., 2003, *ApJ*, **593**, 661
- Weinberger R., et al., 2017, *MNRAS*, **465**, 3291
- Weinberger R., Springel V., Pakmor R., 2020, *ApJS*, **248**, 32
- Wise J. H., Regan J. A., O'Shea B. W., Norman M. L., Downes T. P., Xu H., 2019, *Nature*, **566**, 85
- Wolcott-Green J., Haiman Z., Bryan G. L., 2011, *MNRAS*, **418**, 838
- Wu X.-B., et al., 2015, *Nature*, **518**, 512
- Zhu Q., Li Y., Li Y., Maji M., Yajima H., Schneider R., Hernquist L., 2020, arXiv e-prints, p. arXiv:2012.01458
- Zjupa J., Springel V., 2017, *MNRAS*, **466**, 1625